PLZT Film Waveguide Mach–Zehnder Electrooptic Modulator

G. H. Jin, *Member, IEEE*, Y. K. Zou, *Senior Member, IEEE, Member, OSA*, V. Fuflyigin, S. W. Liu, Y. L. Lu, J. Zhao, and M. Cronin-Golomb, *Member, OSA*

***Abstract*—We report the numerical analysis and the fabrication of a reversed-ridge PLZT film waveguide. It is single-mode, has low transmission loss, and has large transverse cross-section suitable for efficient coupling to single-mode optical fibers. We used this structure to fabricate Mach–Zehnder (MZ) waveguide modulators. The field distribution in the channel and Y branch waveguides was calculated using a beam propagation method to analyze the modal profiles and the propagation loss. The reversed-ridge waveguides and the MZ structures were fabricated on r-sapphire substrates with a patterned ITO spacer film by sol-gel deposition. At 1.55 μm the propagation loss was 2.7 dB/cm. In the MZ, the half-wave modulation voltage was 8.5 V using 1.55μm light and electrode length of 3.5 mm.**

***Index Terms*—Beam propagation method (BPM), lanthanum-doped lead zirconate titanate (PLZT) film, large single-mode profile, Mach–Zehnder (MZ) modulator, reverse-ridge waveguide, sol-gel deposition.**

I. Introduction

THERE has been considerable interest in developing ferroelectric thin films for integrated optoelectronic (OE) devices because these films have several advantageous physical characteristics. Potential applications include low-voltage electrooptical (EO) modulators [1], compact low-threshold gain devices [2], and switches [3]. The large index difference between film and substrate also leads to strong confinement of waveguides, thus allowing the dimensions of the devices to be quite small. Lanthanum-doped lead zirconate titanate (PLZT) [(Pb, La) (Zr,Ti)O_3], has been a very interesting thin film material for optical waveguide devices due to its excellent functional properties, such as piezoelectricity, pyroelectricity, and EO effects. Several methods of PLZT deposition including electron beam evaporation, ion beam deposition, radio frequency (RF)-planar magnetron sputtering, pulsed laser deposition, and sol-gel deposition, have previously been investigated [4]–[7]. Some thin film waveguide devices such as total internal reflection switches and modulators have been studied [3], [7], [8], [16]. However, these PLZT film waveguide devices still had high propagation loss and small mode profiles that are difficult to match to optical fibers. In these waveguides, the thickness of thin film waveguide had to be less than half a micron to ensure single-mode behavior in both the core and side-regions of channel waveguide. Also, the usual method of etching the PLZT film to form the waveguide ridge leads to severe roughness on both the top surface and sidewalls. This roughness causes high scattering loss, becoming especially severe during beam splitting in Mach–Zehnder (MZ) interferometers. To the best of our knowledge, low-loss and large profile single-mode film waveguides have not been achieved for functional devices. In this paper, we report the numerical analysis and the fabrication of a relatively large profile single-mode PLZT film waveguide with reversed-ridge structure incorporated into Y-branches and MZ EO waveguide modulators.

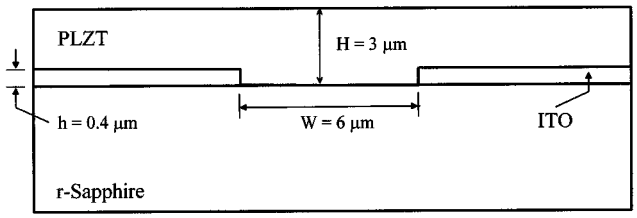

Fig. 1. Schema of the PLZT reversed ridge of waveguide.

II. Analysis and Numerical Simulation

A. Large Profile Single-Mode Reversed-Ridge PLZT Film Waveguides

Fig. 1 shows the reversed-ridge waveguide structure. The PLZT waveguide is deposited on top of a thin photolithographically patterned ITO spacer film. The main reason to use the reversed-ridge structure is that by etching the spacer film instead of the PLZT film we can significantly reduce the surface roughness of the waveguide. In conventional ridge waveguides, the formation of ridges by etching leads to roughness both on the sidewalls and the waveguide surfaces next to the ridge. As is well known, light scattering from surface roughness is the main source of propagation loss. In the reversed-ridge film waveguide, however, the roughness on the horizontal surfaces of waveguide next to the ridge is determined by the spacer film deposition procedure, so that low roughness ($\sigma < 10$ nm) may be ensured. The resultant waveguide surfaces are much smoother than those produced by etching procedures. Another advantage of the reversed-ridge structure is that the effect of the roughness is less than for a regular ridge waveguide, since the difference in refractive index

Manuscript received September 24, 1998; revised October 15, 1999. This work is supported by National Scientific Foundation of USA under the Award ECS-9423666 and by DARPA SBIR phase II program under the Contract "DAAH 01-95-c-R205".

G. H. Jin, Y. L. Lu, and M. Cronin-Golomb are with the Center of Electro-Optics Technology, Tufts University, Medford, MA 02155 USA.

Y. K. Zou, V. Fuflyigin, S. W. Liu, and J. Zhao are with the NZ Applied Technologies, Woburn, MA 01801 USA.

Publisher Item Identifier S 0733-8724(00)05069-6.

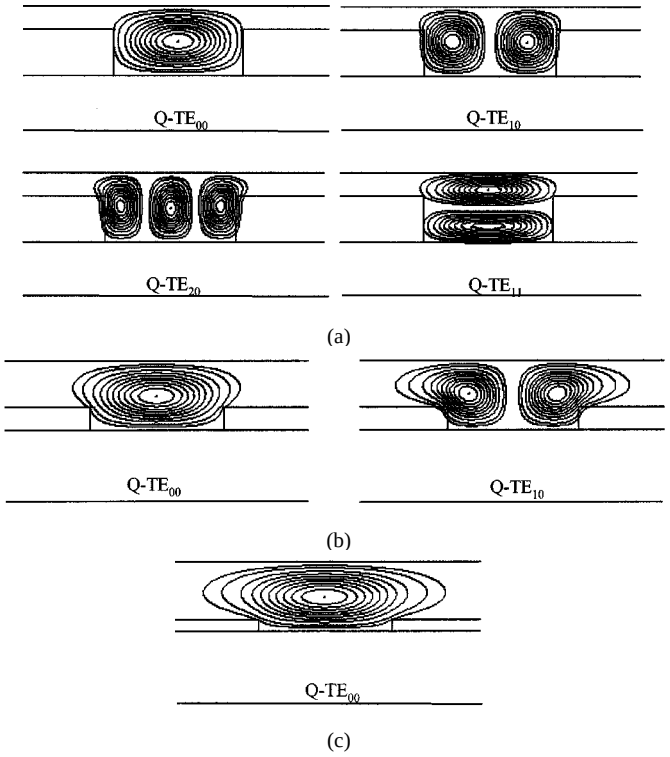

Fig. 2. (a) Modal profiles at 2 μm high reverse-ridge of waveguide. (b) Modal profiles at 1 μm high reverse-ridge of waveguide. (c) Modal profiles at 0.4 μm high reverse-ridge of waveguide.

between the spacer and PLZT is less that between PLZT and air. In this work, we used r-cut sapphire substrates, ITO deposited film as the spacer, and 3-μm-thick PLZT film as guiding layer. According to planar waveguide theory the high refractive index difference we have between the guiding layer and substrate $(\Delta n \sim 0.3)$ would force a single-mode waveguide to be less than 0.5-μm thick. Therefore, it would seem impossible to form single-mode channel waveguides using such a high index difference $(\Delta n \sim 0.3)$ and 3-μm thick film. However, the fact is that large cross-section single-mode waveguides with high refractive index differences have been fabricated in silicon-on-insulator structure [9], [10]. The reason is that there may be mode coupling from higher-order planar guiding modes in the core region to low-order modes in the regions next to the core. This leads to leakage of higher order modes in the core to radiation modes in the outside planar region. Mode-coupling theory may be used on the reversed-ridge waveguide to approximately determine the waveguide structure. A more accurate analysis would numerically resolve the mode equation in two dimensions to get the modal profiles and mode effective indices. In our work, the beam propagation method (BPM) [11]–[13] was used to study the effect of varying the ridge height on the modal profiles of 3-μm high by 6-μm wide PLZT film waveguides. First, as shown in Fig. 2(a), four modes were obtained for $h = 2$ μm. (See Fig. 1). They are the first, second, and third horizontal modes and second vertical mode. The multiple horizontal modes arise because the ridge provides strong lateral confinement for the fundamental and second planar mode within the ridge. The higher order planar modes $(m = 2 \ldots 7)$ disappeared because of leakage to the radiation

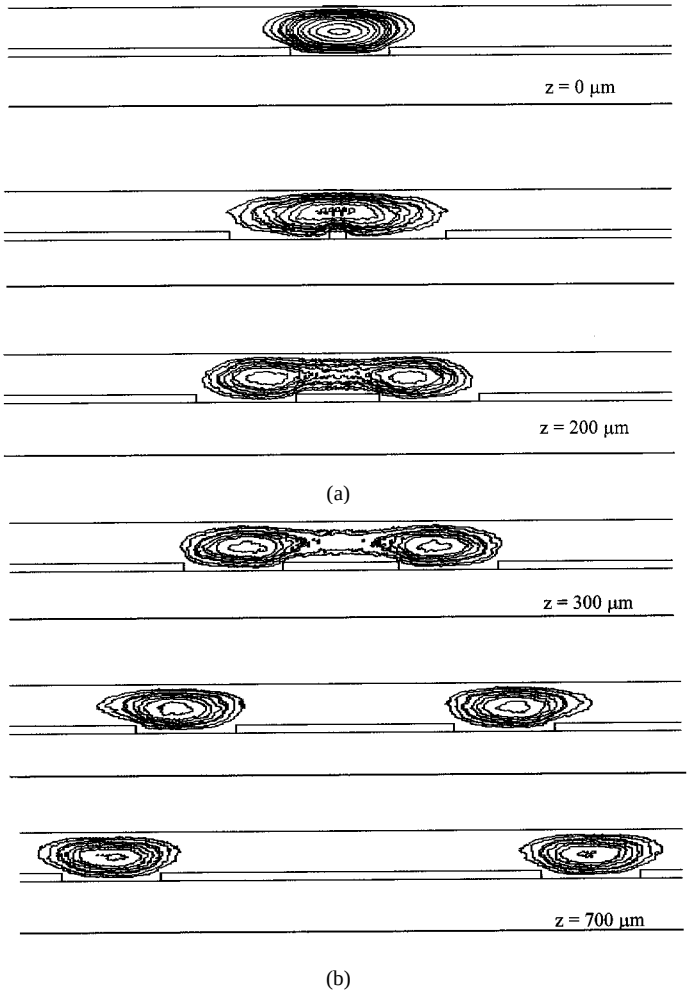

Fig. 3. Optical intensity distribution along the Y-branch waveguide.

mode. As the ridge height decreases from 2 μm to 0.5 μm, the lateral confinement becomes weaker so the lower order modes start to radiate away. For example, as shown in Fig. 2(b), in the case of 1.0 μm high ridge, the fourth transverse electric $(TE)_{01}$ and third TE_{20} mode disappeared. Finally, for ridge heights less than or equal to 0.5 μm, only the fundamental mode exists as shown in Fig. 2(c). Meanwhile, the lateral size of fundamental mode becomes wider as the height of the ridge decreases. This effect can be used to improve the mode matching between the optical fiber and the waveguide. Similar results can be achieved for thicker PLZT films to further improve the mode matching.

B. Numerical Simulation of Optical Field in Y-Branch Waveguide

The MZ interferometer is a very commonly used structure in integrated optoelectronics. Generally, the directional coupler or Y-branch is used for the required beam splitters and combiners. For simplicity of structure and short optical path, we preferred to use the Y-branch. We simulated light propagation in the Y type beam splitter shown in the inset of Fig. 4 using a three–dimensional (3-D)-BPM [12]. We used 6 μm wide and 0.4 μm high reversed-ridge waveguides as described above. Fig. 3 shows our calculation of the optical intensity profiles along the direction of propagation in the Y-structures. As the light propagates the

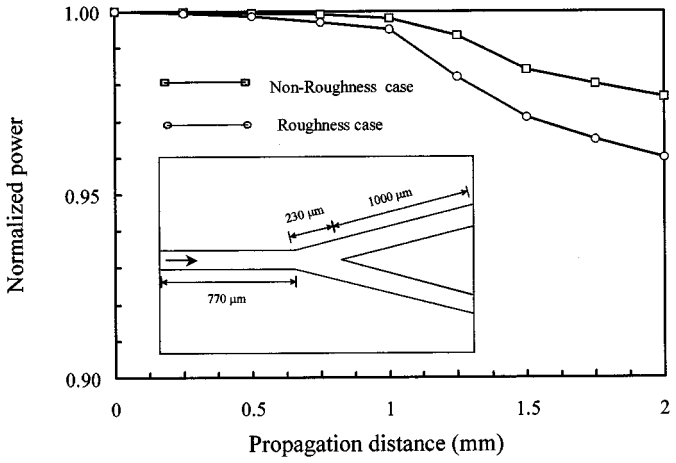

Fig. 4. Normalized optical power versus the propagation distance in the 1.5° intersection angle of Y-branch waveguides.

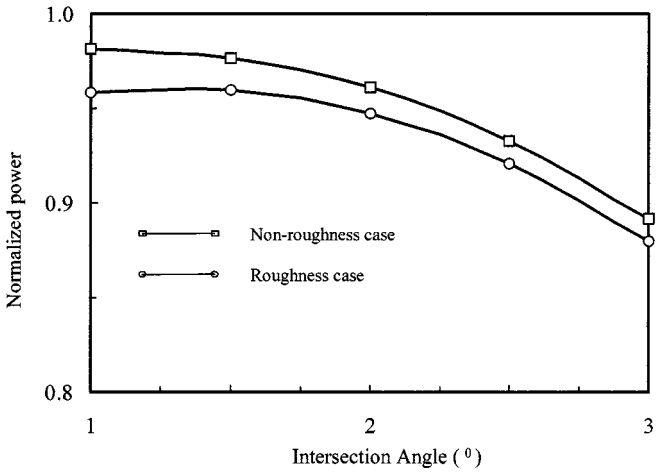

Fig. 5. Normalized power on function of the intersection angle after 2 mm of propagation in Y-branch waveguide.

single-mode profile adapts first to the tapered width, then divides progressively into the two arms of the Y-branch. Notice, in particular, that a significant amount of light is distributed in the area between the two branches. Therefore, we expected that roughness on the surfaces between the channels of the Y-branch would lead to much stronger scattering light than that in straight channel waveguides. Using a numerical scattering model [14] in the beam propagation model, we made a simple comparative analysis of propagation losses in the Y-branch for two cases. In one case, we calculated splitting losses when the waveguide elements were taken to be perfectly smooth. In the other case we set 80 nm standard deviation roughness (σ) only on the horizontal surface between ITO spacer and PLZT films. Here, we only consider light scattering on the horizontal surface, because the roughness difference on these surfaces between the normal and reversed-ridge waveguides is much more than that on etched sidewalls of ridge. Fig. 4 gives the normalized total optical power as a function of propagation distance in a Y-branch with 1.5° intersection angle. In this calculation, the first 0.77 mm of propagation was in a straight waveguide, then 0.23 mm of propagation in the taper and finally 1 mm of propagation in the two arms of the Y-branch. In the first case, propagation loss only came from radiation due to the mode mismatch from the straight waveguide to the tilted one. In the case of the rough waveguide, propagation loss in the single straight waveguide section appeared because of scattering. Then, in the beam splitting step (from 1 to 1.25 mm), the propagation loss was significantly increased compared to the first curve. The relatively more optic distribution between the two branches results in this stronger scattering. As another comparison, in Fig. 5, we show the calculated propagation losses as a function of the Y-branch intersection angle in the both the smooth and rough cases. In the case of the smooth waveguide, the smaller the intersection angle of Y, the smaller the radiation losses due to mode mismatch. However, in the case of the waveguide with surface roughness, the propagation loss was higher for a 1° intersection angle Y-branch than for the 1.5° Y-branch because of more scattering loss during beam splitting. As the roughness increases, the scattering loss increases. Moreover, for a smaller intersection angle a longer Y-branch is needed to separate the MZ waveguides sufficiently, resulting in increased scattering loss. In summary, it is necessary to choose the intersection angle appropriately to effect a compromise between mode mismatching loss and scattering loss in real MZ waveguide structures. Reversed-ridge waveguides have significant advantages when it comes to reducing scattering losses in Y branches because their horizontal surfaces are smoother than those of etched ridge waveguides.

III. Fabrication of Single-Mode Waveguides and MZ Structure

A. Fabrication Process

The reversed-ridge waveguide shown in Fig. 1 was fabricated by first depositing a 0.4-μm-thick transparent ITO film on an r-cut sapphire substrate. The RMS surface roughness of this thick ITO was less than 1 nm from AFM measurements. The thickness was chosen to result in a single mode waveguide as determined by our beam propagation model. Straight and Y branch waveguides, as well as MZ structures were patterned on the ITO film by photolithography and etching. PLZT film with a thickness of 3 μm was then deposited on the patterned ITO/sapphire using a sol-gel deposition technique developed by NZAT [15]. This technique allows the growth of thick uniform large-area films of PLZT. The PLZT film growth temperature and speed were respectively 750 °C and 100 nm/dip. X-ray diffraction indicated that the PLZT films had $\langle 110 \rangle$ pure phase normal to the plane of film. The RMS surface roughness was less than 2.5 nm according to AFM measurements. The quadratic EO coefficient of the PLZT film was measured to be 0.25×10^{-16} (m/V)^2 at 632.8 nm under an external electrical field of $\sim 10^6$ V/m, smaller than the value 1.0×10^{-16} (m/V)^2 which was gotten in thin film (<0.4 μm) by Adachi and Wasa [16]. The dielectric constant was measured to be about 1000 for the PLZT films. The surfaces of the PLZT film on top of the reversed-ridge were examined using a microscope and a SEM at the cleaved waveguide edges. No V-type depression of surface on top of the reversed-ridges was observed under our conditions of 0.40-μm-thick ITO film

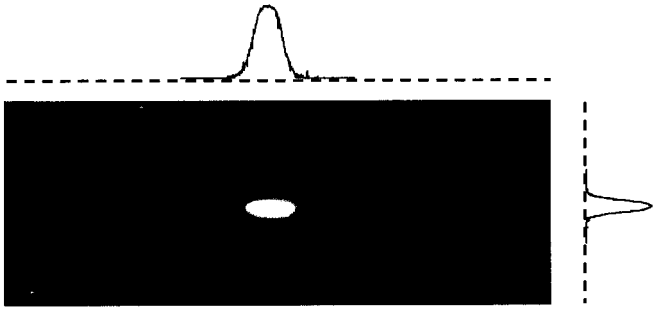

Fig. 6. Near optical field image and scanned intensities from the straight waveguide for 1.55 μm light.

and 3-μm-thick PLZT film. Apparently, the shallow channel fills in uniformly when the PLZT guiding layer was grown by the sol-gel process.

B. Optical Characterization

In the first step of optical characterization, the straight and Y branch waveguides were tested at a wavelength of 1.55 μm. The waveguides were cleaved into 3, 5, 10, and 15 mm lengths respectively for characterization. Diode laser light was injected into the channel waveguides by a single-mode optic fiber ($D \sim 8$ μm). The near field optical distribution was imaged from the output facet of waveguides using an IR camera. In order to check all possible modes in the waveguide, different alignments between the input optic fiber and the straight waveguide were used to excite the fundamental mode as well as higher modes if they exist. The near-field distributions imaged from the output facet of waveguides were also scanned in two orthogonal directions. One of the near field images from a straight waveguide is shown in Fig. 6 together with transverse optical intensity scans. With all the various coupling positions and alignment angles between the injecting fiber and the straight channel waveguide, the optical images had almost the same single-peaked profile at 1.55 μm as that shown in Fig. 6. In no case could we discern any higher order modes in the output of the waveguides. We could not checkout the high-order modes from the near-field distribution images at the output facet of waveguides for all samples. These results verified that the large cross-section reversed-ridge waveguide as designed by numerical calculation had yielded single-mode propagation. In addition, from the measurements of mode profile, we calculated the coupling efficiency between the single-mode fiber and the reversed-ridge waveguide using the following relation:

$$\xi = \frac{|\int E_i E_j^* \, ds|^2}{\int E_j E_j^* \, ds \int E_i E_i^* \, ds} \tag{1}$$

where $E_{i,j}$ are the mode profiles in optic fiber and channel waveguide respectively. The coupling efficiency ξ of the reversed-ridge waveguide would be about 0.656 (-1.83 dB), five times more than that ($\xi \sim 0.125$) of a 0.5-μm-thick single-mode ridge waveguide.

In Fig. 7, we presented one of the near field images from a 1.5° of Y-branch waveguide. The power ratio in the two branches is 1:0.98, so that the corresponding extinction coefficient will be about 18.2 dB for an MZ interferometer. The

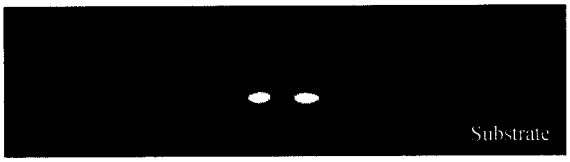

Fig. 7. Near optical field image coming out from the Y-branch waveguide for 1.55 μm light.

difference of optical power in the two arms may be due to imperfections of the etched waveguide pattern on the ITO film. By measuring the intensity reduction in scattered light along the length of the waveguide, we estimated the propagation loss of the waveguides to be about 2.7 ± 0.6 dB/cm. We also measured the loss to be about 4.2 ± 0.8 dB/cm at 1.3 μm laser wavelength. The reduction of the Rayleigh scattering efficiency as the wavelength increases was supposed to be the main reason that the propagation loss decreases at longer wavelength [1]. The throughput for 10 mm straight waveguide and 1.55 μm wavelength was measured to be -7.1 dB. Total losses (7.1 dB) came from three parts, one was the propagation loss ($\sim$2.7 dB), second was the reflection loss ($\sim$1.80 dB) caused by reflections at the two cleaved surfaces of waveguide, the rest ($\sim$2.6 dB) was considered as the coupling loss due to the mode mismatch between the single-mode fiber and the waveguide, and the radiation of high-order modes.

IV. MZ Electrooptic Waveguide Modulator

A. Fabrication

An MZ electrooptic waveguide modulator photolithographically patterned as described above. Electrodes were deposited on the space between two arms as well as at the sides of the waveguides in the MZ interferometer. The electrode gap was 10 μm and the central electrode width was 20 μm. The effective length of the modulation electrodes was 3.5 mm. Platinum was used as electrode material in sputter deposition. We made two different structures so that we could investigate the electrical characteristics of PLZT film for further research on the traveling wave EO waveguide modulators. The first structure had a 0.2 μm thick SiO_2 buffer layer under the electrodes. The second structure was made without a SiO_2 buffer layer. The capacitance of the structure with the SiO_2 layer (29.2 pf) is much less than that without the buffer layer (124.5 pf) because of the large difference between the dielectric constants of PLZT film and SiO_2. This will significantly affect the electric field distribution and frequency response in the modulator.

B. EO Modulation Characterization

In this step of the work, we characterized optical intensity modulation in the MZ PLZT film waveguide modulator. Zero voltage was loaded at the central electrode, then the modulating voltages V_1 ($=V_b+V_m$), V_2 ($=V_b-V_m$), where $V_b = 20$ v, were respectively loaded on other electrodes, see the Fig. 8(a). From the measurements of I_{out} versus V_m, we obtained half-wave voltages of 35.4 V and 8.5 V for the modulator with and without the SiO_2 buffer layer respectively. The electrical field in the waveguide with the buffer layer was about four times weaker

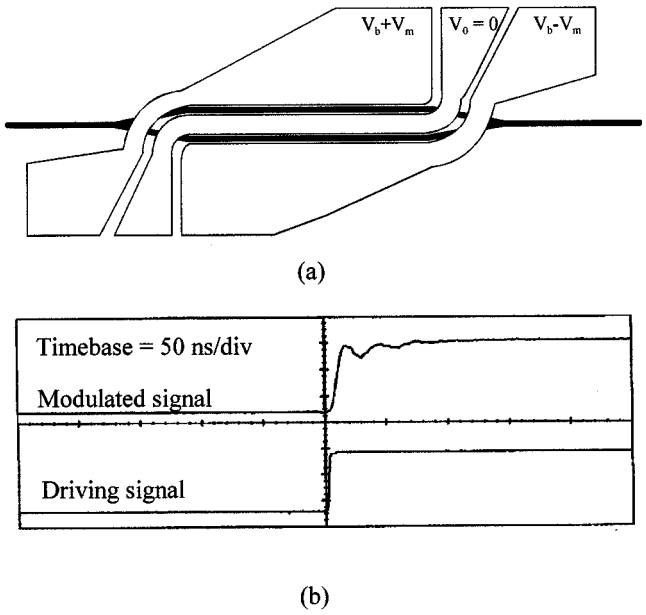

Fig. 8. (a) Scheme of the PLZT waveguide EO modulator. (b) Measurement of the respond time.

TABLE I
CHARACTERISTICS OF PLZT MACH ZEHNDER MODULATOR WITH AND WITHOUT SiO_2 BUFFER LAYER AT 1.55 μm WAVELENGTH

	With SiO_2 buffer layer	Without SiO_2 buffer layer
Modulation depth at 1kHz	0.93	0.93
Modulation depth at 2MHz	0.91	0.89
Rise time	5ns	15ns
Half wave voltage	35.4V	8.5V

than in the case without the buffer layer because the potential was mainly loaded on the buffer layer with its low dielectric constant. The increase in the half-wave voltage will be the main obstacle to the use of a buffer layer for reducing speed mismatch in a traveling wave PLZT waveguide modulator. By measuring the maximum and minimum output optical intensities $(I_{\max}, I_{\min})$, the extinction ratio Γ and the modulation depth M were calculated to be about 14.4 dB and 0.93 in each case at 1 kHz. The modulation depth decreased from 0.93 at 1 kHz to 0.89 at 2 MHz for the modulator without the SiO_2 buffer layer, and from 0.93 at 1 kHz to 0.91 at 2 MHz for the modulator using SiO_2 buffer layer. The response times were less than 5 ns and 15 ns for the modulators with and without the buffer layer respectively, when the rising from 0 to 90% of full amplitude of optic signal was taken as the response time. Table I summarized the results measured in the 3-μm-thick waveguide MZ-modulator with 10 μm gap of electrodes using 1.55 μm wavelength of laser. One of the response time measurements is shown in Fig. 8(b) for a modulator without the buffer layer. Evidently, to improve the response time, we will need to decrease the capacitance by optimizing the modulator electrodes.

V. CONCLUSION

In this paper, we reported the use of the reversed-ridge waveguide structure in the numerical analysis, fabrication, and the demonstration of low-loss, relatively large profile single-mode PLZT film waveguides. We also fabricated and characterized PLZT MZ waveguide modulators using the same reversed-ridge principle. The numerical analysis allowed us to obtain modal profiles for a variety of different waveguides. We also showed that roughness on the horizontal surfaces of waveguide next to ridge greatly increases the scattering loss along the Y-branch section during the beam splitting. Here, the reversed-ridge structure has a significant advantage because the deposition process of the spacer film results in smoother horizontal waveguide surfaces than can be obtained by the standard etching process. We fabricated 3-μm thick PLZT film single-mode reversed-ridge waveguides and Y-branches, in which the coupling efficiency between an optical fiber and the waveguide could be about 0.66. This is about five times more than that of a normal thin film ridge waveguide. The propagation loss at 1.55 μm was 2.7 dB/cm. Our short (3.5 mm) MZ waveguide EO modulators had an extinction ratio of 14.4 dB and half-wave voltage of 8.5 V at 1.55 μm. These results show the potential of reversed-ridge oxide film waveguides for low-voltage, high confinement modulators with good mode matching to optical fibers.

REFERENCES

[1] D. M. Gill, C. W. Conard, G. Ford, B. W. Wessels, and S. T. Ho, "Thin film channel waveguide electro-optic modulator in epitaxial $BaTiO_3$," *Appl. Phys. Lett.*, vol. 71, pp. 1783–1785, 1997.
[2] G. N. van den Hoven, R. J. I. Koper, A. Polman, C. van Dam, J. W. M. van Uffelen, and M. K. Smit, "Net optical gain at 1.53 mum in Er-doped Al2O3 waveguides on silicon," *Appl. Phys. Lett.*, vol. 68, pp. 1886–1888, 1996.
[3] H. Higashino, T. Kawaguchi, H. Adachi, T. Makino, and O. Yamazaki, "High speed optical TIR switch using PLZT thin film waveguides," *Japan. J. Appl. Phys.*, vol. 24, pp. 284–286, 1985.
[4] M. Ishida, H. Matsunami, and T. Tanaka, "Preparation and properties of ferroelectric PLZT thin film by sputtering," *J. Appl. Phys.*, vol. 48, pp. 951–956, 1977.
[5] M. Okuyama, T. Uski, and Y. Hamakawa, "Epitaxial growth of ferroelectric PLZT thin film and their optical properties," *Appl. Phys.*, vol. 21, pp. 339–345, 1980.
[6] P. F. Baude, C. Ye, T. Tamagama, and D. L. Polla, "Fabrication of sol-gel derived ferroelectric $Pb_{0.865}La_{0.09}Zr_{0.65}Ti_{0.35}O_3$ optical waveguides," *J. Appl. Phys.*, vol. 73, pp. 7960–7962, 1993.
[7] S. B. Xiong, Z. G. Liu, X. Y. Chen, X. L. Guo, and X. Liu, "Pulsed laser deposition and characterization of optical waveguiding (Pb, La)(Zr,Ti)O_3 thin film," *Appl. Phys. Lett.*, vol. 67, pp. 2729–2731, 1995.
[8] T. Kawaguchi, H. Adachi, K. Setsune, O. Yamazaki, and K. Wasa, "PLZT thin film waveguides," *Appl. Opt.*, vol. 23, pp. 2187–2191, 1984.
[9] R. A. Soref, J. Schmidtchen, and K. Petermann, "Large single-mode rib waveguides in GeSi-Si and Si-on SiO_2," *IEEE J. Quamtum Electron.*, vol. 27, pp. 1971–1974, 1991.
[10] J. Schmidtchen, B. Schuppert, A. Splett, and K. Petermann, "Low loss rib-waveguide in SOI," *Mater. Res. Soc. Symp. Proc.*, vol. 244, pp. 351–355, 1992.
[11] G. Ronald Hadley and R. E. Smith, "Full-vector waveguide modeling using an iterative finite-difference method with transparent boundary condition," *J. Lightwave. Technol.*, vol. 13, pp. 465–499, 1995.
[12] H. Deng, G. H. Jin, J. Harari, J. P. Vilcot, and D. Decoster, "Investigation of 3-D semivectorial finite-difference beam propagation method," *J. Lightwave Technol.*, vol. 16, pp. 915–922, 1998.
[13] J. C. Chen and S. Jungling, "Computation of high-order waveguide modes by imaginary-distance beam propagation method," *Optic. Quantum Electron.*, vol. 26, pp. 199–205, 1994.

[14] G. H. Jin, J. Harari, J. P. Vilcot, and D. Decoster, "Numerical analysis of the radiation losses due to surface roughness in integrated optical devices," *IEEE Photon. Technol. Lett.*, vol. 8, pp. 1202–1204, 1996.
[15] V. Fuflyigin, K. K. Li, F. L. Wang, H. Jiang, S. W. Liu, J. Zhao, and P. Norris *et al.*, "Preparation of ferroelectric oxide films by sol-gel method," in *High-Temperature Superconductors and Novel Inorganic Materials*, V. Tendeloo *et al.*, Eds. New York: Kluwer Academic, 1999, pp. 279–284. printed in the Netherlands.
[16] H. Adachi and K. Wasa, "Sputtering preparation of ferroelectric PLZT thin film and their optical applications," *IEEE Trans. Ultrason., Ferroelect., Freq. Contr.*, vol. 38, pp. 645–655, 1991.

G. H. Jin (M'97), photograph and biography not available at the time of publication.

Y. K. Zou (SM'94), photograph and biography not available at the time of publication.

V. Fuflyigin, photograph and biography not available at the time of publication.

S. W. Liu, photograph and biography not available at the time of publication.

Y. L. Lu, photograph and biography not available at the time of publication.

J. Zhao, photograph and biography not available at the time of publication.

M. Cronin-Golomb, photograph and biography not available at the time of publication.